

H α IMAGING WITH *HUBBLE SPACE TELESCOPE*-NICMOS OF AN ELUSIVE DAMPED Ly α CLOUD AT $z = 0.6^1$

NICOLAS BOUCHÉ

Department of Astronomy, University of Massachusetts, LGRT 531, Amherst, MA 01003; bouche@nova.astro.umass.edu

JAMES D. LOWENTHAL

Department of Astronomy, University of Massachusetts, LGRT 526, Amherst, MA 01003; james@astro.umass.edu

JANE C. CHARLTON

Department of Astronomy and Astrophysics, Pennsylvania State University, University Park, PA 16802; charlton@astro.psu.edu

MATTHEW A. BERSHADY

Department of Astronomy, University of Wisconsin, Madison, 475 North Charter Street, Madison, WI 53076-1582; mab@astro.wisc.edu

CHRISTOPHER W. CHURCHILL

Department of Astronomy and Astrophysics, Pennsylvania State University, University Park, PA 16802; cwc@astro.psu.edu

AND

CHARLES C. STEIDEL

California Institute of Technology, Palomar Observatories, Pasadena, CA 91125; ccs@astro.caltech.edu

Received 2000 September 6; accepted 2000 November 21

ABSTRACT

Despite previous intensive ground-based imaging and spectroscopic campaigns and wideband *Hubble Space Telescope* (*HST*) imaging of the $z = 0.927$ QSO 3C 336 field, the galaxy that hosts the damped Ly α system along this line of sight has eluded detection. We present a deep narrowband H α image of the field of this $z_{\text{abs}} = 0.656$ damped Ly α absorber, obtained through the F108N filter of NICMOS1 on board the *HST*. The goal of this project was to detect any H α emission 10 times closer than previous studies to unveil the damped absorber. We do not detect H α emission between 0".05 and 6" (0.24 and 30 h^{-1} kpc) from the QSO, with a 3σ flux limit of $3.70 \times 10^{-17} h^{-2} \text{ ergs s}^{-1} \text{ cm}^{-2}$ for an unresolved source, corresponding to a star formation rate (SFR) of $0.3 h^{-2} M_{\odot} \text{ yr}^{-1}$. This leads to a 3σ upper limit of $0.15 M_{\odot} \text{ yr}^{-1} \text{ kpc}^{-2}$ on the SFR density, or a maximum SFR of $1.87 M_{\odot} \text{ yr}^{-1}$ assuming a disk of 4 kpc in diameter. This result adds to the number of low-redshift damped Ly α absorbers that are not associated with the central regions of Milky Way-like disks. Damped Ly α absorption can arise from high-density concentrations in a variety of galactic environments including some that, despite their high local H I densities, are not conducive to widespread star formation.

Subject headings: galaxies: evolution — galaxies: formation — galaxies: high-redshift —
quasars: absorption lines — quasars: individual (3C 336)

1. INTRODUCTION

QSO absorption lines provide a powerful approach to studying the history of galaxies. The nature of damped Ly α absorbers (DLAs) toward background QSOs has been an ongoing debate for more than a decade. Wolfe et al. (1986, 1995) proposed that DLAs are large progenitors of today's massive spiral disks. Evidence in support of this interpretation includes the measurement of absorption-line velocity profiles that are consistent with those expected from lines of sight intercepting rotating, thick gaseous disks (Prochaska & Wolfe 1997). However, recent theoretical simulations of galaxy formation showed that a large range in structures (e.g., halo gas clouds) and morphologies, rather than a single uniform type of galaxy, can give rise to DLAs (e.g., Katz et al. 1996; Haehnelt et al. 1998; McDonald & Miralda-Escudé 1999). In this case, they could be low surface brightness (LSB), gas-rich, dwarf galaxies as proposed by Tyson (1988) and more recently by Jimenez et al. (1999).

DLAs make up the largest reservoir of neutral hydrogen (H I) at high redshift (Wolfe et al. 1986; Lanzetta et al. 1991; Rao & Turnshek 2000). There are hundreds of DLAs, defined as absorbers with atomic hydrogen column densities $N(\text{H I})$ greater than $2 \times 10^{20} \text{ cm}^{-2}$, known up to redshifts $z \sim 4$. From the redshift distribution of the measured column densities of the damped systems, the evolution of neutral gas density [$\Omega_{\text{DLA}}(z)$] can be measured (Lanzetta et al. 1991, 1995; Wolfe et al. 1995; Storrie-Lombardi et al. 1996; Rao & Turnshek 2000). The analysis of the variation of $\Omega_{\text{DLA}}(z)$ with redshift can provide another measurement of the evolution of the star formation rate in the universe (Pei & Fall 1995). Rao & Turnshek (2000) find little evolution in $\Omega_{\text{DLA}}(z)$ from $z = 4$ to $z = 1$. Over this interval we might have expected a decrease in Ω_{DLA} as the gas is converted into stars in order to maintain the observed constant star formation rate (Steidel et al. 1999). This led Rao & Turnshek (2000) to conclude that DLAs and the galaxies that dominate the star formation density are different populations.

Furthermore, it is difficult to reconcile the low metallicities of high-redshift DLAs (typically 1/10 of solar at $z \sim 2.5$; Pettini et al. 1997) with the higher metallicities of stars in galaxies today: no chemical evolution is seen in DLAs from $z = 3.5$ to $z = 0.3$ (Pettini et al. 1999), which

¹ Based on observations with the NASA/ESA *Hubble Space Telescope* obtained at the Space Telescope Science Institute, which is operated by Association of Universities for Research in Astronomy, Inc., under NASA contract NAS 5-26555.

indicates that DLAs do not necessarily trace the population responsible for the bulk of star formation. Finally, high-resolution Keck spectra of three QSOs by Pettini et al. (2000) indicate that DLAs ($z < 1.0$) have heterogeneous chemical properties.

Another approach to understanding DLAs is to compare them with current local H I surveys (Rao & Briggs 1993; Zwaan et al. 1999; J. Rosenberg 2000, private communication), which sample neutral gas clouds and galaxies perhaps analogous to distant DLAs (of course, high-redshift and low-redshift DLAs may be produced by very different galaxy populations). Current results (Zwaan et al. 1999; Rao & Turnshek 2000) indicate that local H I samples contain a much smaller fraction of high column densities ($N_{\text{HI}} > 10^{21} \text{ cm}^{-2}$) than both low- and high-redshift DLAs. These results imply strong evolution at the highest column densities. However, estimates of the local column density distribution rely on many caveats, such as the true nature of the debated local H I mass function. Beam smearing in these H I surveys may also lead to underestimates of the local number of high column density systems, particularly if such regions are physically small.

Prior to 1993, most observations of DLAs were restricted to high-redshift systems ($z > 1.8$) since the Ly α line is in the rest-frame UV. Previous attempts to detect emission from DLAs have concentrated on Ly α (e.g., Lowenthal et al. 1995; see Roche, Lowenthal, & Woodgate 2000 for a summary), which is expected to be a signature of a star-forming region, although its emission may be suppressed by dust extinction. Of at least 10 DLAs at $z \gtrsim 2$ searched for Ly α emission, only a very few show confirmed detections (Djorgovski et al. 1996; Fynbo, Burud, & Møller 2000). Ground-based surveys (photometric and spectroscopic) for H α emission around $z > 2$ DLAs have also been mostly unsuccessful (Bunker et al. 1999; Teplitz, Malkan, & McLean 1998), except in some cases (Bechtold et al. 1998; Mannucci et al. 1998).

Only recently, with the advent of rest-UV spectroscopy from *Hubble Space Telescope* (HST), have data on intermediate-redshift $0.3 < z < 1.8$ DLA systems become available (Le Brun et al. 1997; Boissé et al. 1998). These DLAs display a wide range of morphologies and surface brightnesses. Using NICMOS-NIC2, Kulkarni et al. (2000) reported a possible H α detection of a $z_{\text{abs}} = 1.89$ DLA toward LBQS 1210 + 1731 and Pettini et al. (2000) detected an edge-on low-luminosity $L \sim \frac{1}{6} L^*$ galaxy 10 kpc away from the QSO 0058 + 019 ($z_{\text{abs}} = 0.612$) using WFPC2. In addition, ground-based observations such as WIYN images of three low-redshift DLAs ($z < 0.3$) show dwarf and/or low surface brightness hosts, with confirmed redshifts (Rao & Turnshek 1998; Lane et al. 1998).

In contrast, the larger class of Mg II absorbers with $3 \times 10^{17} \leq N(\text{H I}) \leq 2 \times 10^{20} \text{ cm}^{-2}$ (Lyman limit systems) are almost always associated with fairly luminous ($L_K > 0.05 L_K^*$) galaxies, i.e., within $35 h^{-1} \text{ kpc}$ (Steidel et al. 1995). It was once thought that these different classes of absorbers sample different cross-sectional regions of broadly the same galaxies (Steidel et al. 1993), with the DLAs associated with the inner, denser regions. This is only partially true. Dwarf and LSB galaxies apparently can produce DLA absorption at low-impact parameters; however, they do not contribute a significant cross section for Lyman limit absorption.

These issues motivate the current attempts to image DLAs at low impact parameter and, at the same time, might

explain why most previous attempts have failed to reveal gas-rich spirals.

In this paper, we present an HST study of an intermediate-redshift DLA ($z_{\text{abs}} = 0.656$) along the line of sight toward QSO 3C 336 ($z = 0.927$) that has, so far, eluded detection entirely despite extensive ground-based searches (Steidel et al. 1997). This QSO line of sight is one of the richest known for $z < 1$ absorption-line studies, with six metal-line systems in the interval $0.317 < z < 0.892$. For that reason this quasar field was the target of both a very deep 24,000 s HST-WFPC2 image and a 2160 s Keck/NIRC image (Steidel et al. 1997). Five galaxies associated with the metal-line systems were identified in the WFPC2 image and their redshifts confirmed spectroscopically using the Keck/LRIS (Steidel et al. 1997). The only unidentified absorber is a DLA at $z = 0.656$ with $N(\text{H I}) = 2 \times 10^{20} \text{ cm}^{-2}$ and $[\text{Fe}/\text{H}] = -1.2$. There is no galaxy detected ($L > 0.05 L_K^*$) near the QSO line of sight and as close as $0'.5$ ($\sim 2 h^{-1} \text{ kpc}$). Two unlikely candidate galaxies exist at large impact parameters from the QSO. The first is a relatively faint, $M_K = -21.43$ ($m_K = 20.77$), late-type spiral located $14'.3$ ($\sim 65 h^{-1} \text{ kpc}$) northeast of the QSO. Taking into account the estimated disk inclination and the position angle, Steidel et al. (1997) estimated it would require a disk extent of at least $\sim 120 h^{-1} \text{ kpc}$ to intercept the QSO line of sight. The second candidate is a galaxy without a confirmed redshift. If one assumes this galaxy is at the redshift of the DLA, it would have an impact parameter of $41 h^{-1} \text{ kpc}$ and $L_B = 0.04 L_B^*$ (similar to that of the SMC).

This raises the question of whether DLA absorption can arise in dense H I regions far from the centers of galaxies, perhaps in regions that have little or no current star formation, as seen locally in mergers (Hibbard & Yun 1999) and as pointed out by Rao & Turnshek (2000). Alternatively, a separate absorbing galaxy could be situated beneath the QSO on the plane of the sky.

The goal of this project was to detect any H α emission as close as $\sim 0'.05$ ($0.24 h^{-1} \text{ kpc}$) of the QSO to test further the alternate hypothesis. H α at the redshift of this DLA matches one narrowband filter of the HST-NICMOS camera 1 and, therefore, enables us to put strong constraints on the SFR of the absorber. We can already say there is no L^* spiral galaxy close to the line of sight, for Steidel et al. (1997) did not find anything brighter than $0.05 L_K^*$. On the other hand, one might expect a dwarf or LSB galaxy with significant star formation such as found by Le Brun et al. (1997, 1998) and Rao & Turnshek (2000) for other DLAs.

In the next section, we describe the observations and the reduction of the data. The results are given in § 3, and we compare them with previous studies in § 4. Our conclusions are presented in § 5. Throughout this paper, we adopt $\Omega_M = 0.3$, $\Omega_\Lambda = 0.7$, and $H_0 = 100 h \text{ km s}^{-1} \text{ Mpc}^{-1}$; thus $1''$ at $z = 0.656$ corresponds to $4.85 h^{-1} \text{ kpc}$.

2. OBSERVATIONS AND DATA REDUCTION

2.1. Observations

The observations were carried out with the Near Infrared Camera and Multi-Object Spectrometer (NICMOS) using camera 1 (NIC1) with camera 2 (NIC2) in attached parallel mode on 1997 October 3. NIC1 ($0'.043 \text{ pixel}^{-1}$) was chosen to enable us to oversample the point-spread function (PSF) (FWHM ~ 2 pixels or $0'.09$) and hence to

resolve emission as close as possible to the QSO. The exposure times were 2.8 hours (5 orbits) and 0.7 hours for the filters F108N and F110M, respectively (details are listed in Table 1). The pixel size is $0''.043$, which at the redshift of the DLA corresponds to a physical size of $\sim 0.21 h^{-1}$ kpc pixel $^{-1}$.

For NIC1, we used the narrowband (NB) F108N filter ($\lambda_c = 1.081 \mu\text{m}$; FWHM = $0.0094 \mu\text{m}$) and the broadband (BB) F110M filter ($\lambda_c = 1.101 \mu\text{m}$; FWHM = $0.19 \mu\text{m}$). F108N was chosen to match the wavelength of $\text{H}\alpha$ at the redshift of the DLA ($z = 0.656$), and the BB filter was chosen to subtract continuum emission. For NIC2, the filter F160W ($\lambda_c = 1.596 \mu\text{m}$; FWHM = $0.400 \mu\text{m}$) was chosen, but unfortunately the field turned out to be in an especially empty region of the WFPC2 field (Steidel et al. 1997). The NIC2 images will not be discussed further here.

A reference star (GSC 2044.810 from the STScI Guide Star Catalog) to measure the PSF was chosen within $100''$ of QSO 3C 336. GSC 2044.810 has colors $J-H \sim 0.6$ and $H-K \sim 0.6$, which are similar to that of a typical QSO at $z \sim 1$, i.e., $B-V = 1.05$ and $V-J = 1.68$ (Hyland & Allen 1982). The star ($V = 12.59$) is ~ 5.5 mag brighter than the QSO, which allowed us to shorten exposure times.

Five dithered images of both the QSO and the reference star were taken in both NB and BB filters in order to improve the sampling of the PSF and to avoid any systematic noise from the detector. Each exposure was taken in the MULTIACCUM mode, which allows 25 nondestructive readouts over the entire dynamic range for each pixel. This allows improved cosmic-ray rejection. Exposures were chosen to be short enough to avoid detector saturation.

2.2. Data Reduction

The images of the QSO and the reference star were reduced, shifted, and co-added with the Nired² package (McLeod 1997). The zeroth read was subtracted from each raw image to remove any pedestal level, and dark subtraction was performed using the pipeline dark files provided by STScI. The photon arrival rate in each pixel was computed by fitting a straight line to the MULTIACCUM readouts. Cosmic rays were rejected by searching for a jump between successive readouts so that full information for each pixel is recovered. The images were then flat-fielded with the pipeline flat files provided by STScI. A sky frame was constructed from the dithered observations and subtracted from the images. Each image was magnified by a factor of 2 after masking the residual cosmic rays and bad pixels. Finally, the dithered images were registered and co-added—with a weight proportional to the inverse noise in a reference region close to the QSO image—to produce the final image (hereafter “high S/N” images). The final result improved the S/N by a factor of ~ 8 compared to images

² See <http://cfa-www.harvard.edu/castles/Nired> for more information.

TABLE 1
EXPOSURE TIMES FOR EACH FILTER

Object	F108N (s)	F110M (s)
3C 336	5×2050	5×511
GSC 2044.810	5×303	6×23
GSC 2044.810		5×14

reduced by the STScI pipeline *calnica* process. The FWHM of the PSF is 4.17 pixels (in the magnified images), which corresponds to $0''.090$.

In order to perform absolute photometry on the QSO flux, i.e., to use the multiplying factors (PHOTFLAM) provided by STScI and to convert counts to flux units, we reduced the data using the dark and flat files listed as the Reference Files (used in the calibration of the P330E and G191-B2B 7691 data) prescribed by the NICMOS handbook v. 3.0 (hereafter “calibrated” images). To check for any correlation noise produced by the magnification process, we reduced the data without magnifying the pixels (hereafter “small calibrated” images) with the same dark and flat files and we confirmed our noise figures (measured around the QSO) in the calibrated images. In the NB QSO field, the S/N was ~ 125 and ~ 15 , respectively, for the high S/N, and *calnica* images. In the small calibrated and calibrated images, the S/N was ~ 95 . We used the high S/N images for PSF subtraction, while the noise properties were measured in the calibrated images. The calibrated image is shown in Figure 1.

2.3. Photometry and Noise Properties

The total fluxes were obtained by measuring the curve of growth for each of the calibrated QSO images. We converted the fluxes measured within $0''.5$ radius aperture to nominal infinite aperture fluxes by multiplying them by 1.15 as prescribed by STScI.³

³ See <http://www.stsci.edu/cgi-bin/nicmos/> under *documents* and *handbooks*. See also Figs. 4.6–4.10 from the NICMOS Instrument Handbook v3.0, chapter 4.

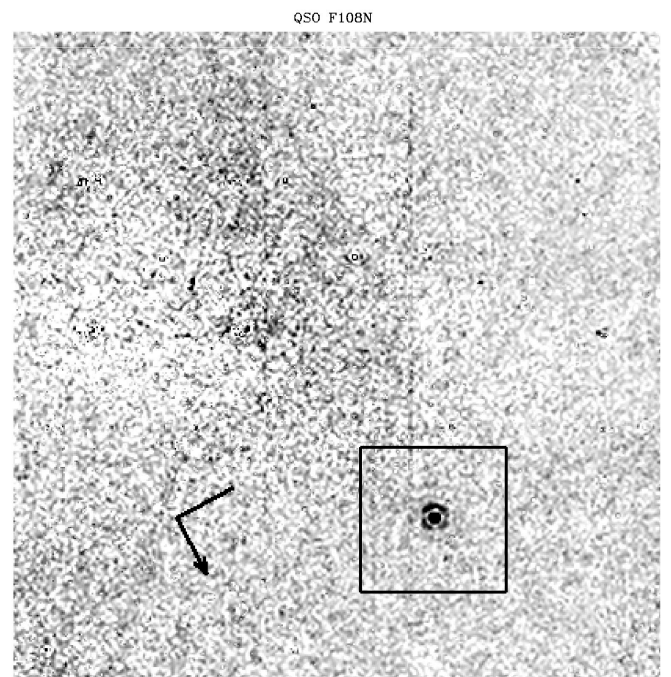


FIG. 1.—Calibrated NIC1 narrowband F108N image of the $11'' \times 11''$ field around QSO 3C 336. The box is $2'' \times 2''$ and centered on the QSO. The arrow indicates north. The image is shown in reverse: dark is positive flux.

In the NB calibrated image, the noise beyond the PSF is constant within a 2'' radius circle (from 10 to 50 pixels) around the QSO. Beyond a radius of 2'', the noise increases as a result of the poorer first quadrant of the NICMOS detector.

Our 3 σ detection limit for a point source is given by the 3 σ rms per resel (a resel or resolution element is a 0''.09 diameter aperture, corresponding to the FWHM of the PSF) measured in the quadrant of the image that includes the QSO. For the NB image, our 3 σ detection limit is $F_\lambda = 3.78 \times 10^{-19}$ ergs s⁻¹ cm⁻² Å⁻¹ [$m_{AB} = 23.48$, where $m_{AB} = -2.5 \times \log(F_\nu) - 48.6$], or a flux of $F_{H\alpha} = 3.70 \times 10^{-17}$ ergs s⁻¹ cm⁻². For the BB image, our 3 σ detection limit is $F_\lambda = 2.9 \times 10^{-20}$ ergs s⁻¹ cm⁻² Å⁻¹ ($m_{AB} = 26.22$), or a flux of $F_{BB} = 5.82 \times 10^{-17}$ ergs s⁻¹ cm⁻².

Our 3 σ detection limits for an extended source are given by the 3 σ rms per pixel scaled by the square root of the number of pixels in a 1'' \times 1'' square. The resulting limits are 4.70×10^{-18} ergs s⁻¹ cm⁻² Å⁻¹ ($m_{AB} = 20.75$) in the NB image and 3.60×10^{-19} ergs s⁻¹ cm⁻² Å⁻¹ ($m_{AB} = 23.49$) in the BB image. These correspond to surface brightnesses of 4.60×10^{-16} ergs s⁻¹ cm⁻² arcsec⁻² for the NB image and 7.17×10^{-16} ergs s⁻¹ cm⁻² arcsec⁻² for the BB image.

The total flux densities of the QSO in the NB and the BB are $(4.55 \pm 0.18) \times 10^{-17}$ ergs s⁻¹ cm⁻² Å⁻¹ ($m_{AB} = 18.3$) and $(5.09 \pm 0.17) \times 10^{-17}$ ergs s⁻¹ cm⁻² Å⁻¹ ($m_{AB} = 18.1$), respectively. These results are summarized in Table 2.

2.4. Profile Subtraction

In order to reveal any faint object with small impact parameter, we subtracted the QSO PSF in the following ways:

To search for faint emission both close to the QSO line of sight and throughout the 11'' field, we first subtracted the BB QSO image (scaled to the peak value) from the NB QSO image. The central part, shown on Figure 2, panel *a*, has faint residuals (negative and positive peaks well below 3 σ) near the QSO position. The total residual flux measured in a resel centered on the QSO is about 1.5 σ above the mean or 0.7% of the (unsubtracted) NB QSO flux in the same aperture.

To assess how much of those residuals might be because of differences in PSF between the F108N and F110M filters and how much to real H α flux from a dwarf galaxy exactly superposed on the QSO position, we used the same procedure (i.e., shifting and centering) to subtract the BB PSF from the NB PSF of the reference star (GSC 2044.810). We find residuals with a similar pattern (see Fig. 2, panel *b*). There is clearly a peak near the center with a depression above and below (in the *y*-direction). The stellar PSF residual pattern on larger scales is not seen in the QSO PSF subtracted image, since the S/N is more than 10 times lower. The central peak pixel in the residuals is about 1.5% the flux of the stellar PSF peak, while the magnitude of the deepest depression is about -5% of the stellar PSF peak. The total residual flux measured in a resel centered on the position of the star is 0.7% of the NB stellar PSF flux in the same aperture, consistent with the QSO residuals. Therefore, we conclude the residuals are likely due to PSF differences between the two filters.

Because the stellar NB-BB method described above produced such significant residuals, we then tried subtracting a stellar PSF (scaled to the peak) directly from the QSO high S/N image. This was performed for both the NB and BB filters. We used both a theoretical PSF generated by the

TABLE 2
SUMMARY OF RESULTS IN QSO 3C 336 FIELD

Parameter	Value
QSO ($z = 0.927$)	
R.A., decl. (J2000).....	16 ^h 24 ^m 39 ^s .13, +23°45'11".7
F_λ (1.08 μm) (ergs s ⁻¹ cm ⁻² Å ⁻¹).....	$(4.55 \pm 0.18) \times 10^{-17}$
$m_{AB,1.08\mu\text{m}}$ (mag).....	18.28 ± 0.1
F_λ (1.10 μm) (ergs s ⁻¹ cm ⁻² Å ⁻¹).....	$(5.09 \pm 0.17) \times 10^{-17}$
$m_{AB,1.10\mu\text{m}}$ (mag).....	18.11 ± 0.1
3 σ Upper Limits on Continuum Emission at $z = 0.656$	
F_λ (1.10 μm) (ergs s ⁻¹ cm ⁻² Å ⁻¹).....	$< 2.92 \times 10^{-20}$
$m_{AB,1.10\mu\text{m}}$ (mag).....	< 26.22
F_{BB} (unresolved source) (ergs s ⁻¹ cm ⁻²).....	$< 5.82 \times 10^{-17}$
L_R (unresolved source) (h^{-2} ergs s ⁻¹).....	$< 5.02 \times 10^{40}$
3 σ Upper Limits on H α Emission from the Damped Ly α Cloud ($z = 0.656$)	
F_λ (1.08 μm) (ergs s ⁻¹ cm ⁻² Å ⁻¹).....	$< 3.78 \times 10^{-19}$
$m_{AB,1.08\mu\text{m}}$ (mag).....	< 23.48
$F_{H\alpha}$ (point source) (ergs s ⁻¹ cm ⁻²).....	$< 3.70 \times 10^{-17}$
$L_{H\alpha}$ (point source) (h^{-2} ergs s ⁻¹).....	$< 3.20 \times 10^{40}$
\Rightarrow SFR (point source) ($h^{-2} M_\odot \text{ yr}^{-1}$).....	< 0.28
$\mu_{H\alpha}$ (3 σ) (ergs s ⁻¹ cm ⁻² arcsec ⁻²) ^a	$< 4.60 \times 10^{-16}$
$\Sigma_{H\alpha}$ (h^{-2} ergs s ⁻¹ arcsec ⁻²) ^b	$< 3.98 \times 10^{41}$
$\Sigma_{H\alpha}$ (ergs s ⁻¹ kpc ⁻²) ^b	$< 1.67 \times 10^{40}$
\Rightarrow Surface SFR ($M_\odot \text{ yr}^{-1} \text{ kpc}^{-2}$).....	< 0.15
\Rightarrow SFR ($r = 2$ kpc disk) ($M_\odot \text{ yr}^{-1}$).....	< 1.87

^a H α surface brightness.

^b H α surface luminosity.

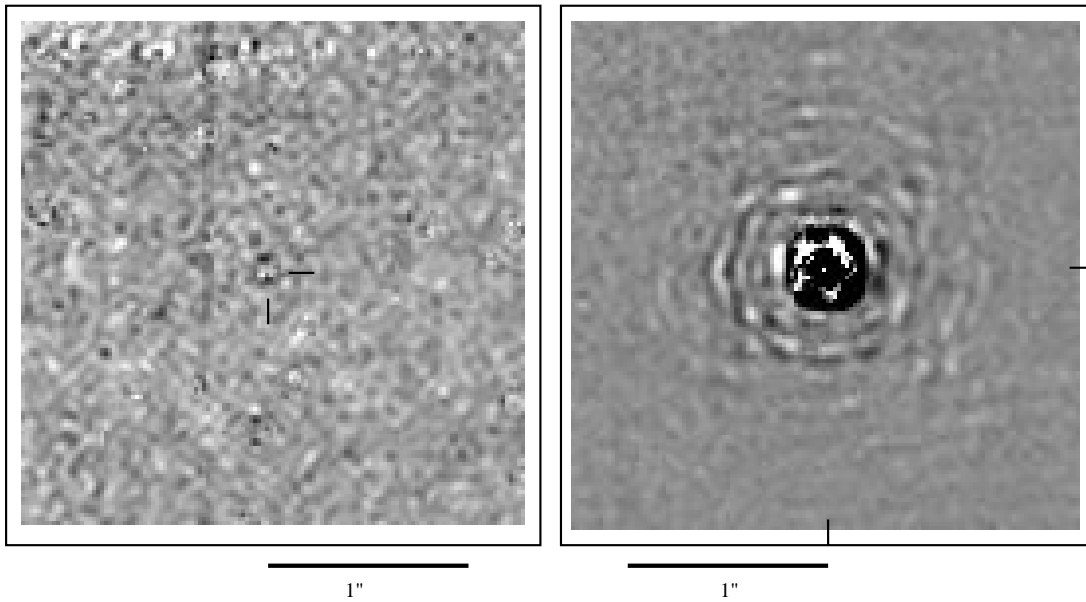


FIG. 2.—*Left*: Narrowband NIC1 image of the QSO field after subtraction of broadband NIC1 image. Images were registered and scaled to the peak value prior to subtraction. Residual flux in 1 resel at the QSO position is only 1.5σ above the mean. The original position is shown by the tick marks. *Right*: Same for the reference star. Note the significant residual flux pattern, which is consistent with the QSO residuals, although at much higher signal-to-noise ratio. In both images, positive flux is shown as white.

software Tiny Tim (J. Krist et al. 1997,⁴ adapted by Richard Hook for NICMOS) and the reference star (GSC 2044.810) PSF. Unfortunately, the reference star turns out to be double, i.e., after the subtraction, a PSF-like hole was seen in both NB and BB images offset by $0''.17$ from the central PSF (see Fig. 3, panel *a*). We corrected for this by subtrac-

⁴ The program and information are available online at <http://www.stsci.edu/software/tinytim>.

ting the primary component of the star PSF from the secondary component, and then subtracted the result from the QSO PSF. The final result shows very little residual (see Fig. 3, panel *b*). However, when using the theoretical PSF instead, the result tends to leave a ringlike structure. For this reason, we adopted the stellar PSF as the best approximation of the true PSF. The final PSF subtracted NB image is shown in Figure 3, panel *b*, after a Gaussian smoothing of 1.5 pixels.

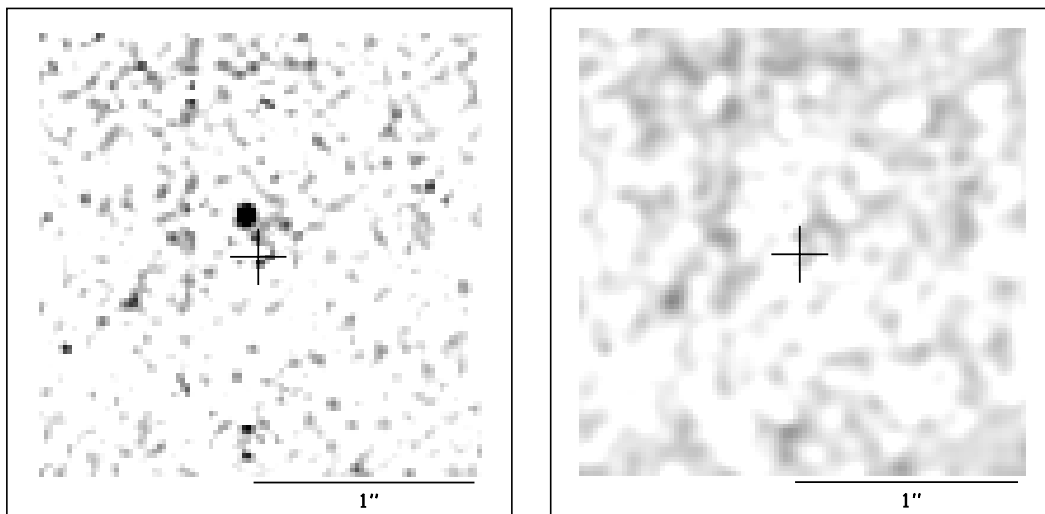


FIG. 3.—*Left*: Blow up of $2'' \times 2''$ around the QSO after subtraction of the scaled star PSF. The cross marks the position of the QSO. The star turns out to be a close double, resulting in a “hole” $0''.17$ from the QSO. *Right*: Same as (*left*) after second PSF subtraction to remove the stellar companion. Image has been smoothed to 1.5 pixel resolution to enhance any extended emission. No residual flux is detected. (*left*) and (*right*) are the “high S/N” images and positive emission is in white.

Finally, in the NB PSF subtracted image, we looked for faint emission throughout the 11" field both by eye and using the algorithm SExtractor (Bertin & Arnouts 1996) with a 3σ threshold (with a minimum of 16 pixels above threshold, i.e., the keyword MINAREA in SExtractor). Three candidates were found. Every candidate was followed up by examining individual images and it turned out that all candidates were artifacts left over from the reduction process, e.g., cosmic-ray residuals smeared out over several pixels by the magnification process.

3. RESULTS AND DISCUSSION

To summarize, we looked for emission objects near the QSO and throughout the field in the following way: (1) We subtracted the BB image from the NB image. Apart from residuals due to PSF differences between the two filters, no emission was detected. (2) We subtracted the star PSF from the QSO PSF in both NB and BB images. No emission was detected. (3) We searched by eye for any faint emission throughout the 11" field in both the NB PSF subtracted and the "NB minus BB" images. (4) In the NB PSF subtracted image, we also used the algorithm SExtractor (Bertin & Arnouts 1996) to look for faint emission. All three candidates were cosmic-ray residuals smeared out over several pixels. Therefore, we conclude that no emission objects were detected either in the NB PSF subtracted or in the "NB minus NB" image.

We can use the lack of detection in the BB image to constrain the presence of luminous galaxies. The BB 3σ detection limit for a point source is $m_{AB} = 26.22$, which corresponds to a continuum luminosity of $L_R = 5.02 \times 10^{40} h^{-2} \text{ ergs s}^{-1}$ in the rest frame R band or $L_R = 7.23 \times 10^7 h^{-2} L_\odot$.

In addition, our lack of detection in the NB constrains directly the SFR. For the NB filter, our 3σ detection limit for a point source (i.e., unresolved) corresponds to an $H\alpha$ luminosity of $3.20 \times 10^{40} h^{-2} \text{ ergs s}^{-1}$ at the redshift of the DLA. The 3σ detection limit for an extended source corresponds to an $H\alpha$ luminosity of $3.98 \times 10^{41} h^{-2} \text{ ergs s}^{-1} \text{ arcsec}^{-2}$ at the redshift of the DLA (see Table 2). Using the Kennicutt (1983) conversion factor for a constant SFR and a modified Salpeter-like IMF with variable slope, i.e., $\text{SFR} = L_{H\alpha}/1.12 \times 10^{41} \text{ ergs s}^{-1}$, we derive a SFR of less than $0.28 h^{-2} M_\odot \text{ yr}^{-1}$ for an unresolved source or less than $0.15 M_\odot \text{ yr}^{-1} \text{ kpc}^{-2}$ for an extended source. Assuming the absorber is a disk of radius 2 kpc (i.e., ~ 9 times the resolution element; see discussion below), this gives a SFR of less than $1.87 M_\odot \text{ yr}^{-1}$.

More recently, the calibration of Kennicutt (1998) yields a similar conversion factor $\text{SFR} = L_{H\alpha}/1.26 \times 10^{41} \text{ ergs s}^{-1}$. Our upper limit is a conservative one given that the actual SNR in the magnified images used in the subtraction process is higher than the calibrated images and that the conversion factor is the smallest of current estimates. The SFR estimate is also dependent on the IMF. Using a Salpeter initial mass function with a higher mass cutoff ($125 M_\odot$), Alonso-Herrero et al. (1996) found $\text{SFR} = L_{H\alpha}/3.1 \times 10^{41} \text{ ergs s}^{-1}$, which is about 3 times larger than the Kennicutt (1983) result. This would decrease our upper limit by a factor of 3, i.e., a SFR less than $0.6 M_\odot \text{ yr}^{-1}$ for a 2 kpc radius disk.

This estimate depends strongly on the assumed size of the object. However, from Steidel et al. (1997), there cannot be any $L > 0.05L^*$ galaxy (typically 10 kpc in size) as close as

$0''.5$ ($2 h^{-1} \text{ kpc}$). In other words, anything larger than 4 kpc (in diameter) would have been seen in both Steidel et al. (1997) and in our images. A 2 kpc radius object is consistent with the size of the DLA candidate ($z = 1.89$) of Kulkarni et al. (2000). Similarly, Le Brun et al. (1997; see § 4) detect compact objects with sizes of 1–3 kpc along DLA lines of sight. On the other hand, if the absorbing object is smaller, it could have a higher SFR. This would require that it be smaller than 1 resel or $\sim 0.5 \text{ kpc}$, and that it be exactly aligned with the line of sight of the QSO.

4. COMPARISON WITH PREVIOUS STUDIES

We first discuss our result in the context of previous surveys of DLAs, and then compare our SFR limits to four types of galaxy seen in the local universe.

From *HST* imaging of the fields of seven quasars with DLAs at $0.395 < z < 1.78$, Le Brun et al. (1997) were able to resolve galaxy-like objects at small impact parameters for six of their QSO lines of sight with $0.395 < z < 1.1$. However, the hosts of these DLAs displayed a broad range of morphologies and surface brightnesses: three of the six detections are spirals, two are compact, LSB galaxies, and two others have compact morphologies. Recently, Pettini et al. (2000) reported the detection of an edge-on low-luminosity $M_B = -19.1$ or $L \sim \frac{1}{6}L^*$ galaxy 10 kpc away from the QSO 0058+019 using *HST*-WFPC2. Using NICMOS-NIC2 Kulkarni et al. (2000) reported a possible detection of an $H\alpha$ emission feature, $2\text{--}3 h_{70}^{-1} \text{ kpc}$ in size, $0''.25$ from a $z = 1.89$ DLA. They suggest that a faint, compact, somewhat clumpy object, rather than a thick, spiral disk, is responsible for this DLA. The implied 3σ upper limit on the SFR is $4 h_{70}^{-2} M_\odot \text{ yr}^{-1}$, which applies unless dust obscuration is important. Note that we used the same conversion factor ($L_{H\alpha}/\text{SFR}$) as Kulkarni et al. (2000).

The ground-based spectroscopic survey of Bunker et al. (1999), which searched for redshifted $H\alpha$ emission in $11'' \times 2''.5$ regions around six quasars with $z > 2$ DLAs, reached a 3σ detection limit of $6\text{--}18 M_\odot \text{ yr}^{-1}$ and failed to detect any redshifted $H\alpha$ emission. Some ground-based narrowband photometric surveys (e.g., Teplitz, Malkan, & McLean 1998) for $H\alpha$ emission from DLAs have also failed to detect any emission-line objects in the DLA fields, although Teplitz et al. (1998) found $H\alpha$ emitters in the fields of some weaker non-DLA metal line systems. However, other narrowband searches for $H\alpha$ emission have revealed multiple objects in the DLA fields separated by more than several to tens of arcseconds from the QSO (Bechtold et al. 1998; Mannucci et al. 1998). These surveys, which had 3σ detection limits of $\sim 5\text{--}10 M_\odot \text{ yr}^{-1}$, found these $H\alpha$ -emitting objects to have a wide range of SFRs, $6\text{--}90 M_\odot \text{ yr}^{-1}$. Kulkarni et al. (2000) suggested the relatively large separations of these emission-line objects from the quasar indicate that they are not the DLA absorbers themselves, but star-forming regions in a group or cluster also containing the DLA. None of these ground-based surveys has been able to probe the regions very close ($< 2''$ or 11.7 kpc at $z = 2$) to the quasar line of sight to rule out large spiral disks at high redshift with confidence.

The nature of the DLA toward 3C 336 can be addressed by comparing directly our SFR upper limit to various types of galaxy in the local universe. (1) LSB galaxies have $H I$ surface densities of $\sim 5 M_\odot \text{ pc}^{-2}$ or $N_{HI} \sim 6.5 \times 10^{20} \text{ cm}^{-2}$ (van der Hulst et al. 1993), well above the DLA cutoff of $2 \times 10^{20} \text{ cm}^{-2}$ but below the value of 10^{21} cm^{-2} usually

quoted as the threshold for star formation. The mean star formation rates, derived from the $\text{H}\alpha$ luminosities, in LSBs are typically $\sim 0.1 M_{\odot} \text{ yr}^{-1}$ (van den Hoek et al. 2000). (2) Blue compact dwarf galaxies (BCDGs): From CFHT observations, Petrosian et al. (1997) reported a SFR of $0.3\text{--}0.5 M_{\odot} \text{ yr}^{-1} \text{ kpc}^{-2}$ for the two main $\text{H}\alpha$ emitting regions of the local ($D = 10 \text{ Mpc}$) BCDG, IZW 18; (3) Typical spiral galaxies: The typical SFR for a spiral galaxy is $\sim 10 M_{\odot} \text{ yr}^{-1}$ (van den Hoek et al. 2000), spread over at least several kiloparsecs; (4) Starbursts can have a much larger SFR, e.g., Arp 220 is forming stars at a rate of $\sim 240 M_{\odot} \text{ yr}^{-1}$, derived from $\text{Ly}\alpha$ (Anantharamaiah et al. 2000). The SFR in the DLA at $z = 0.656$ toward 3C 336 is far less extreme than in a starburst or a typical spiral, and somewhat less extreme than a BCDG. However, it is consistent with that of an LSB galaxy and it could be even lower, i.e., zero.

Another example of a region of neutral hydrogen that exceeds the DLA threshold, but does not have significant star formation, has been found through 21 cm observations of the giant H I cloud 1225 + 0146 (Giovanelli & Haynes 1989); these data show that neutral gas structures with little or no star formation do exist. This suggests that factors beyond a simple column density threshold govern the formation of stars. This giant H I cloud is 200 kpc along its major axis and has two peaks of H I emission, with $N(\text{H I}) = 2 \times 10^{20}$ and $1 \times 10^{20} \text{ cm}^{-2}$, separated by 100 kpc. In a deep optical search, only a faint $M_B = -15.5$ dwarf irregular, 5 kpc in extent, was discovered, corresponding to the largest peak in emission (McMahon et al. 1990). Furthermore, no galaxy has been detected near the 10^{20} cm^{-2} peak, which is almost enough neutral hydrogen to produce a DLA.

The absorption-line properties of the DLA toward 3C336 corroborate the observed low SFR. This DLA is unusual in that it is a “C IV–deficient” Mg II absorber—rest-frame equivalent width $W(\text{C IV}) \sim 0.5 \text{ \AA}$ (Steidel et al. 1997)—i.e., $W(\text{C IV})$ is less than half the typical value for DLAs. Churchill et al. (1999) found a correlation between the strength of C IV absorption and the kinematic spread of the Mg II profile in high-resolution absorption profiles, with the exception of several C IV–deficient absorbers. They hypothesize that there is a relationship between the strength of C IV absorption (which is generally consistent with arising in a corona similar to that around the Milky Way disk) and the level of star formation activity in the disk. The kinematic spread of the Mg II profile is also thought to be related to star-forming processes that either eject or are triggered by high-velocity Mg II clouds. In this scenario, the C IV–deficient absorbers would be characterized by a lower than average star formation rate, and in fact a few of them do have red colors (Churchill et al. 2000), rather than the blue colors of actively star-forming systems. This is consistent with the fact that the 3C336 DLA has both a small $W(\text{C IV})$ and a strong limit on the star formation rate in its vicinity.

There is at least some theoretical reason to expect low SFRs from DLAs. Mo, Mao, & White (1999) hypothesize that—at least at $z \sim 3$ —Lyman break galaxies (LBGs), which are selected partly by their strong star formation, and DLAs could be disjoint populations: If LBGs are the central galaxies of massive dark halos at $z \sim 3$, then they should be small objects with substantial star formation but low angular momentum, while DLAs should be biased toward objects with large angular momentum. In the hierarchical structure formation models of Maller et al. (2000),

meanwhile, DLAs arise from the combined effects of massive central galaxies and a number of smaller satellite galaxies in virialized halos, rather than only the central galaxies, so predicted SFRs associated with DLAs are low. Another interesting result from Maller et al.’s models is that the impact parameter distribution has a longer tail at $z \sim 1$ (up to 150 kpc) than at redshift $z \sim 3$, which could then reconcile the observed galaxy 120 kpc away from the line of sight of 3C 336 and the $z = 0.656$ absorber.

5. SUMMARY AND CONCLUSIONS

We can summarize previous observational results on DLAs as follows: (1) DLAs show little evolution of $\Omega(z)$ from $z = 4$ to $z = 1$ (Rao & Turnshek 2000); (2) DLAs show little metallicity evolution (Pettini et al. 1999) from $z = 3$ to $z = 0.3$; (3) $z < 1$ DLAs have heterogeneous chemical properties (Pettini et al. 2000); (4) DLAs have various morphologies (Le Brun et al. 1997; Kulkarni et al. 2000; Rao & Turnshek 2000) (although it is possible that at least some DLAs are large disks like the galaxies found by Le Brun et al. [1997] and Pettini et al. [2000]). These results are inconsistent with the standard DLA/H I disk paradigm (Wolfe et al. 1995), for they indicate that DLAs (1) do not participate in the overall chemical enrichment of the universe and hence do not trace star formation; and (2) are not characteristic of a particular type of galaxy. Rather they are merely characteristic of a particular type of region: namely, one with a large neutral column density (e.g., Khersonsky & Turnshek (1996)). It is quite reasonable, following the results of Rao & Turnshek (2000), to assume that this applies to higher redshift DLAs as well.

Nearly all space-based observations of low-redshift DLAs have revealed star formation in some sort of galaxy. The $z = 0.656$ system toward 3C 336 is an exception. Our lack of detection of any source with SFR greater than $0.28 h^{-2} M_{\odot} \text{ yr}^{-1}$, or $0.15 M_{\odot} \text{ yr}^{-1} \text{ kpc}^{-2}$, demonstrates that DLAs with very little star formation can exist.

As evidence mounts against the standard, DLA/H I disk scenario, we must address the question: “What is a DLA?” Possibilities not yet ruled out include knots of H I hundreds of kiloparsecs away from the main galaxy as seen locally (Hibbard & Yun 1999); small compact dwarfs or LSBs; or photodissociation regions that may produce much of the H I currently observed in galaxy disks (Smith et al. 2000). In some cases, both a cold (hundreds of K) and a warm (thousands of K) neutral medium are found along the line of sight through a DLA, based upon analysis of 21 cm emission profiles (Lane, Briggs, & Smette 2000), while in others the warm phase dominates.

Our limits on $\text{H}\alpha$ emission from the DLA toward 3C 336 set the tightest constraints yet on star formation in a compact absorber at intermediate redshift and probe closer to the QSO line of sight than any previous study. Our nondetection adds to the mounting evidence that low-redshift DLAs are made of galaxies of diverse morphologies, luminosities, and surface brightnesses rather than a uniform population of luminous disk galaxies.

Support for this work was provided by NASA through grant GO-07449.01-96A from the Space Telescope Science Institute, which is operated by the Association of Universities for Research in Astronomy, Inc., under NASA contract NAS 5-26555. M. A. B. acknowledges support from NASA LTSA contract NAG 5-6032.

REFERENCES

- Alonso-Herrero, A., Aragón-Salamanca, A., Zamorano, J., & Rego, M. 1996, *MNRAS*, 278, 417
- Anantharamaiah, K. R., Viallefond, F., Mohan, N. R., Goss, W. M., & Zhao, J. H. 2000, *ApJ*, 537, 613
- Bechtold, J., Elston, R., Yee, H. K. C., Ellington, E., & Cutri, R. M. 1998, in *ASP Conf. Ser. 146, The Young Universe: Galaxy Formation and Evolution at Intermediate and High Redshift*, ed. S. D'Odorica, A. Fontana, & E. Giallongo (San Francisco: ASP), 241
- Bertin, E., & Arnouts, S. 1996, *A&AS*, 117, 393
- Boissé, P., Le Brun, V., Bergeron, J., & Deharveng, J.-M. 1998, *A&A*, 333, 841
- Bunker, A. J., Warren, S. J., Clements, D. L., Williger, G. M., & Hewett, P. C. 1999, *MNRAS*, 309, 875
- Churchill, C. W., Mellon, R. R., Charlton, J. C., Jannuzi, B. T., Kirhakos, S., Steidel, C. C., & Schneider, D. P. 1999, *ApJ*, 519, L43
- . 2000, *ApJ*, 543, 577
- Djorgovski, S. G., Pahre, M. A., Bechtold, J., & Elston, R. 1996, *Nature*, 382, 234
- Fynbo, J. U., Burud, I., & Møller, P. 2000, *A&A*, 358, 88
- Giovanelli, R., & Haynes, M. P. 1989, *ApJ*, 346, L5
- Haehnelt, M. G., Steinmetz, M., & Rauch, M. 1998, *ApJ*, 495, 647
- Hibbard, J. E., & Yun, M. S. 1999, *AJ*, 118, 162
- Hyland, A. R., & Allen, D. A. 1982, *MNRAS*, 199, 943
- Jimenez, R., Bowen, D. V., & Matteucci, F. 1999, *ApJ*, 514, 83L
- Katz, N., Weinberg, D. H., Hernquist, L., & Miralda-Escudé, J. 1996, *ApJ*, 457, 57L
- Kennicutt, R. C., Jr. 1983, *ApJ*, 272, 54
- . 1998, *ARA&A*, 36, 189
- Khersonsky, V. K., & Turnshek, D. A. 1996, *ApJ*, 471, 657
- Kulkarni, V. P., Hill, J. M., Schneider, G., Weymann, R. J., Storrie-Lombardi, L. J., Rieke, M. J., Thompson, R. I., & Jannuzi, B. T. 2000, *ApJ*, 536, 36
- Lane, W. M., Briggs, F. H., & Smette, A. 2000, *ApJ*, 532, 146
- Lane, W., Smette, A., Briggs, F., Rao, S., Turnshek, D., & Meylan, G. 1998, *AJ*, 116, 26
- Lanzetta, K. M., McMahon, R. G., Wolfe, A. M., Turnshek, D. A., Hazard, C., & Lu, L. 1991, *ApJS*, 77, 1
- Lanzetta, K. M., Wolfe, A. M., & Turnshek, D. A. 1995, *ApJ*, 440, 435
- Le Brun, V., Bergeron, J., Boissé, P., & Deharveng, J. M. 1997, *A&A*, 321, 733
- Lowenthal, J. D., Hogan, C. J., Green, R. F., Woodgate, B. E., Caulet, A., Brown, L., & Bechtold, J. 1995, *ApJ*, 451, 484
- Maller, A. H., Prochaska, J. X., Somerville, R. S., & Primack, J. R. 2000, in *ASP 200, Clustering at High Redshift*, ed. A. Mazure, O. LeFèvre, & V. Le Brun (San Francisco: ASP)
- Mannucci, F., Thompson, D., Beckwith, S. V. W., & Williger, G. M. 1998, *ApJ*, 501, 11L
- McDonald, P., & Miralda-Escudé, J. 1999, *ApJ*, 519, 486
- McLeod, B. 1997 in *HST Calibration Workshop*, ed. S. Casertano et al. (Baltimore: STScI), 281
- McMahon, R. G., Irwin, M. J., Giovanelli, R., Haynes, M. P., Wolfe, A. M., & Hazard, C. 1990, *ApJ*, 359, 302
- Mo, H. J., Mao, S., & White, S. D. M. 1999, *MNRAS*, 304, 175
- Pei, Y. C., & Fall, S. M. 1995, *ApJ*, 454, 69
- Pettini, M., Ellison, S. L., Steidel, C. C., & Bowen, D. 1999, *ApJ*, 510, 576
- Pettini, M., Ellison, S. L., Steidel, C. C., Shapley, A. E., & Bowen, D. V. 2000, *ApJ*, 532, 65
- Pettini, M., Smith, L. J., King, D. L., & Hunstead, R. W. 1997, *ApJ*, 486, 665
- Petrosian, A. R., Boulesteix, J., Comte, G., Kunth, D., & Lecoarer, E. 1997, *A&A*, 318, 390
- Prochaska, J. X., & Wolfe, A. M. 1997, *ApJ*, 487, 73
- Rao, S. M., & Briggs, F. H. 1993, *ApJ*, 419, 515
- Rao, S. M., & Turnshek, D. A. 1998, *ApJ*, 500, L115
- . 2000, *ApJS*, 131, 1
- Roche, N., Lowenthal, J. D., & Woodgate, B. E. 2000, *MNRAS*, 317, 937
- Smith, D. A., Allen, R. J., Bohlin, R. C., Nicholson, N., Stecher, T. P. 2000, *ApJ*, 538, 608
- Steidel, C. C. 1993, in *The Environment and Evolution of Galaxies*, ed. J. M. Shull & H. A. Thronson, Jr. (Dordrecht: Kluwer), 263
- Steidel, C. C., Adelberger, K. L., Giavalisco, M., Dickinson, M., & Pettini, M. 1999, *ApJ*, 519, 1
- Steidel, C. C., Dickinson, M., Meyer, D. M., Adelberger, K. L., & Sembach, K. R. 1997, *ApJ*, 480, 568
- Steidel, C. C., Pettini, M., Dickinson, M., & Persson, S. E. 1995, *AJ*, 108, 2046
- Storrie-Lombardi, L. J., McMahon, R. G., & Irwin, M. J. 1996, *MNRAS*, 283, 79L
- Teplitz, H. I., Malkan, M., & McLean, I. S. 1998, *ApJ*, 506, 519
- Tyson, N. D. 1988, *ApJ*, 329, L57
- van den Hoek, L. B., de Blok, W. J. G., van der Hulst, J. M., & de Jong, T. 2000, *A&A*, 357, 397
- van der Hulst, J. M., Skillman, E. D., Smith, T. R., Bothum, G. D., McGaugh, S. S., & de Blok, W. J. G. 1993, *AJ*, 106, 548
- Wolfe, A. M., Lanzetta, K. M., Foltz, C. B., & Chaffee, F. H. 1995, *ApJ*, 454, 698
- Wolfe, A. M., Turnshek, D. A., Smith, H. E., & Cohen, R. D. 1986, *ApJS*, 61, 249
- Zwaan, M. A., Verheijen, M. A. W., & Briggs, F. H. 1999, *Publ. Astron. Soc. Australia*, 16, 100